



## Article

**Cite this article:** Hamann JS, Arney T, Kirkham JD, Wachter P, Gohl K (2024). Antarctic ice-shelf meltwater outflows in satellite radar imagery: ground-truthing and basal channel observations. *Journal of Glaciology* 1–13. <https://doi.org/10.1017/jog.2024.71>

Received: 25 January 2024  
Revised: 3 September 2024  
Accepted: 14 September 2024



**Key words:**

glacier discharge; glaciological instruments and methods; ice shelves; melt – basal; remote sensing

**Corresponding author:**

Jakob Stanley Hamann;  
Email: [jakob.hamann467@gmail.com](mailto:jakob.hamann467@gmail.com)

# Antarctic ice-shelf meltwater outflows in satellite radar imagery: ground-truthing and basal channel observations

Jakob Stanley Hamann<sup>1,2</sup> , Thomas Arney<sup>3,4</sup> , James David Kirkham<sup>4</sup>, Paul Wachter<sup>5</sup> and Karsten Gohl<sup>1</sup>

<sup>1</sup>Alfred Wegener Institute, Helmholtz Centre for Polar and Marine Research, Bremerhaven, Germany; <sup>2</sup>Department of Earth Sciences, Physical Geography, Freie Universität Berlin, Berlin, Germany; <sup>3</sup>School of Ocean and Earth Science, University of Southampton, Southampton, UK; <sup>4</sup>British Antarctic Survey, Natural Environment Research Council, Cambridge, UK and <sup>5</sup>German Remote Sensing Data Center (DFD), German Aerospace Center (DLR), Wessling, Germany

**Abstract**

Ice shelves regulate the flow of the Antarctic ice sheet toward the ocean and its contribution to sea-level rise. Accurately monitoring the basal and surface melting of ice shelves is therefore essential for predicting the ice sheet's response to climatic warming. In this study, we utilize Sentinel-1A synthetic aperture radar satellite imagery combined with shipboard measurements of water temperature and salinity to investigate the presence of surficial meltwater plumes along the Antarctic coastline. Our approach reveals a strong correlation between areas of pronounced low radar backscatter extending from ice shelves and significant decreases in water temperature and salinity, suggesting meltwater-enriched ocean waters. We propose that the low radar backscatter signature of meltwater outflows is caused by stable stratification of the upper water column, driven by density contrasts from buoyant, low-salinity meltwater and surface current shear that reduce Bragg scattering waves. The resulting smooth water surfaces were observed adjacent to the surface expression of deep basal channels, documented in a helicopter survey along part of the Bellingshausen Sea ice edge. We present high-temporal resolution satellite radar as a tool for identifying meltwater release from beneath ice shelves, capable of all-weather, day-and-night imaging.

**1. Introduction**

Antarctica plays a critical role in Earth's climate system. In recent decades, the Antarctic ice sheet has experienced significant mass loss (Shepherd and others, 2018; Otosaka and others, 2023), contributing to rising sea levels (Cazenave and others, 2018) and impacting ocean circulation dynamics (e.g. Gunn and others, 2023; Li and others, 2023) and climate patterns (e.g. Bronselaer and others, 2018). Currently, the dominant mechanisms through which ice is lost from the Antarctic ice sheet are the calving of icebergs and basal melting of its ice shelves (Paolo and others, 2015; Greene and others, 2022) which serve as conduits for over 80% of Antarctic ice sheet flow into the Southern Ocean (Rignot and others, 2013). Ice shelves are floating extensions of the Antarctic ice sheet that fringe the continent's coastlines; they act as buttresses which regulate ice discharge by restraining the flow of grounded ice from the interior to the ocean where it ultimately contributes to sea-level rise (Scambos and others, 2004; Dupont and Alley, 2005; Gudmundsson, 2013; Fürst and others, 2016).

Satellite-derived Antarctic ice-shelf thickness assessments reveal extensive thinning in West Antarctica (Pritchard and others, 2012; Paolo and others, 2015, 2023), driven by widespread intrusions of warm Circumpolar Deep Water onto the continental shelf (Rignot and others, 2019), elevating basal melt rates (Schmidtke and others, 2014) and contributing to grounding-line retreat (Rignot and others, 2014). Recent research has highlighted the potential for enhanced Antarctic meltwater production to slowdown ocean circulation and increase incursions of Circumpolar Deep Water onto the continental shelf in a feedback that could exacerbate Antarctic ice losses (Gunn and others, 2023; Li and others, 2023). These findings underline the importance of monitoring and understanding meltwater dynamics from Antarctic ice shelves.

A distinctive feature of many ice shelves characterized by high rates of localized basal meltwater flux is the occurrence of longitudinal basal channels expressed on the ice-shelf surface (Rignot and Steffen, 2008; Le Brocq and others, 2013; Sergienko, 2013; Alley and others, 2016). These channels are pathways for basal meltwater flux and commonly originate near the grounding line, stretching for several tens of kilometers along the general flow direction of the ice. The presence of basal channels may stabilize ice shelves by concentrating melting within a narrow zone, thereby preventing widespread contact of warm water with the ice-shelf base and decreasing average melt rates across the entire ice shelf (Gladish and others, 2012; Millgate and others, 2013). However, basal channels can also contribute to ice-shelf fracture and can initiate calving and retreat events, which in some circumstances can reduce ice-shelf stability (Rignot and Steffen, 2008; Vaughan and others, 2012; Sergienko, 2013; Dow and

© The Author(s), 2024. Published by Cambridge University Press on behalf of International Glaciological Society. This is an Open Access article, distributed under the terms of the Creative Commons Attribution licence (<http://creativecommons.org/licenses/by/4.0/>), which permits unrestricted re-use, distribution and reproduction, provided the original article is properly cited.

[cambridge.org/jog](https://cambridge.org/jog)



others, 2018; Alley and others, 2019). The formation of basal channels influences the distribution and flow of basal meltwater, thereby affecting melt rates and patterns, which are important variables that control ice-shelf stability (Alley and others, 2024).

Remote-sensing approaches, such as satellite-based observations, offer valuable tools for estimating meltwater discharges from Antarctic ice shelves over vast spatial scales (e.g. Fricker and others, 2021). However, most remote-sensing studies monitor long-term trends in ice mass loss, glacier flow acceleration and grounding-line retreat, providing only indirect estimates of subglacial meltwater contributions to the ocean (e.g. Depoorter and others, 2013; Adusumilli and others, 2020; Rignot and others, 2022; Stokes and others, 2022; Schmidt and others, 2023). Some studies associate meltwater discharge with persistent sensible-heat polynyas, which are detectable using thermal (e.g. Mankoff and others, 2012; Savidge and others, 2023) and microwave (e.g. Markus and Burns, 1993) sensors. In contrast, in situ measurements, such as conductivity–temperature–depth (CTD) profiles, directly capture the physical properties of the water column, including salinity and temperature, allowing for a more accurate detection and quantification of meltwater discharges (e.g. Jenkins and others, 2018).

Direct observations of meltwater discharges often rely on the detection of sediment plumes in the vicinity of glaciers. Sediments are eroded from the underside of glaciers and transported by meltwater, creating turbid plumes visible in optical satellite imagery. While the detection of sediment plumes in optical satellite imagery is a common method for identifying meltwater discharges from glaciers and ice sheets (e.g. Lewis and Smith, 2009; Tedstone and Arnold, 2012; Hudson and others, 2014), its applicability is limited for Antarctic ice shelves. Unlike the Greenland ice sheet, where much of the ice margin terminates through tidewater glaciers that are grounded and actively erode sediment (i.e. no floating extension), Antarctic ice shelves typically melt within the ice-shelf cavity or from sources well upstream of the grounding line (e.g. Rignot and others, 2013). Furthermore, the volumes of sediment-laden subglacial meltwater produced in Antarctica are likely limited compared to environments such as Greenland where surface meltwater can access the bed and significantly enhance erosion rates (Cowton and others, 2012). Consequently, meltwater discharges from Antarctic ice shelves may not always involve substantial sediment transport, making the detection of meltwater discharges by searching for sediment plumes inefficient. Additionally, the use of multispectral imagery in the Antarctic region is challenging due to factors such as frequent cloud cover (e.g. Zhu and Woodcock, 2014; Malek and others, 2017), limited daylight hours during the Austral winter, and the presence of atmospheric aerosols, such as dust, sulfates and sea salts (e.g. Kaufman, 1984), which can hinder the visibility and interpretation of meltwater features. These limitations necessitate the exploration of alternative remote-sensing techniques with appropriate ground-truthing to improve meltwater detection and enhance our understanding of its impact on Antarctic ice shelves.

A powerful alternative to multispectral satellite imagery is synthetic aperture radar (SAR) technology which allows for all-weather and day-and-night imaging (Ulaby and others, 1981). SAR can provide observations at a reliable temporal resolution, making it particularly valuable for monitoring remote areas and regions with frequent cloud cover such as Antarctica. It has proven particularly effective in analyzing ice flow dynamics in Antarctica (Rignot and others, 2011, 2022) and Greenland (Joughin and others, 2010; Sundal and others, 2011), as well as for studying meltwater stored in lakes on the surface of ice shelves (Dirscherl and others, 2021; Li and others, 2021). SAR has also been utilized for detecting sea slicks and assessing physical properties of the ocean surface, which are otherwise difficult to

evaluate (Gade and others, 1998; Gurova and Ivanov, 2011; Alpers and others, 2017).

In this paper, we assess the potential of C-band SAR data to identify meltwater discharges from beneath Antarctic ice shelves as they enter the open ocean. Through analyses of SAR imagery and in situ measurements of water temperature and salinity obtained during two ship-based expeditions in 2022 and 2023, we observe distinct meltwater discharges from two different ice shelves in Antarctica. Our results demonstrate the potential of SAR to identify meltwater release from beneath ice shelves. In addition, a helicopter survey of channels on the Venable Ice Shelf supports results inferred from satellite data and provides first-hand context of the morphology of these features that are most often viewed only from space.

## 2. Methods

During two geoscientific research cruises aboard *RV Polarstern* in 2022 and 2023 (expeditions PS128 and PS134), we conducted opportunistic analyses to identify meltwater discharges from ice shelves. Three study sites were examined: (1) Atka Bay off Ekström Ice Shelf of Dronning Maud Land, East Antarctica, (2) Ronne Entrance southwest edge of the George VI Ice Shelf in the eastern Bellingshausen Sea Embayment, West Antarctica and (3) Venable Ice Shelf in the western Bellingshausen Sea Embayment (Fig. 1). We investigated anomalies initially identified in SAR imagery with ship-based thermo-salinity measurements and helicopter aerial imagery.

### 2.1 Detection of meltwater from signatures in SAR imagery

SAR uses microwave pulses emitted from an airborne or spaceborne platform to create images of the Earth's surface by analyzing the phase and amplitude of the reflected signal. It has the advantage of all-weather and day-and-night imaging capabilities. *RV Polarstern* expeditions receive almost daily SAR imagery from the TerraSAR-X satellite, provided directly by the German Aerospace Center, and Sentinel-1A satellite images for assessing sea-ice conditions. Sentinel-1A operates in the C-band frequency with a noise equivalent sigma zero of  $-22$  dB. Historical Sentinel-1A SAR data are available on Copernicus Open Access Hub (<https://scihub.copernicus.eu/>). Each image received during *RV Polarstern* expeditions PS128 and PS134 was calculated to normalized radar backscatter (sigma nought), applying the standardized formula of SAR Level-1 Radiometric Calibration:

$$\text{value}(i) = \frac{|DN_i|^2}{A_i^2} \quad (1)$$

Here,  $\text{value}(i)$  is the calibrated backscatter value,  $DN_i$  is the digital number from the SAR image and  $A_i$  is the sigma nought value from the calibration Look-Up Table, which applies a range-dependent gain. To convert these values to decibels (dB), the following transformation was applied:

$$\text{Sigma Nought (dB)} = 10 \times \log_{10}(\text{Sigma Nought}) \quad (2)$$

The images were then visually inspected for anomalies in backscatter characteristics – indicating changes in surface properties – with particular attention paid to areas of low radar backscatter, a potential indicator of sea slicks that can arise from upwelling of relatively cool ocean water (e.g. Kozlov and others, 2012; Gurova and others, 2013). Identification criteria included plume-like, elongated low backscatter features extending from the ice-shelf front. We focused on areas with broad, consistent

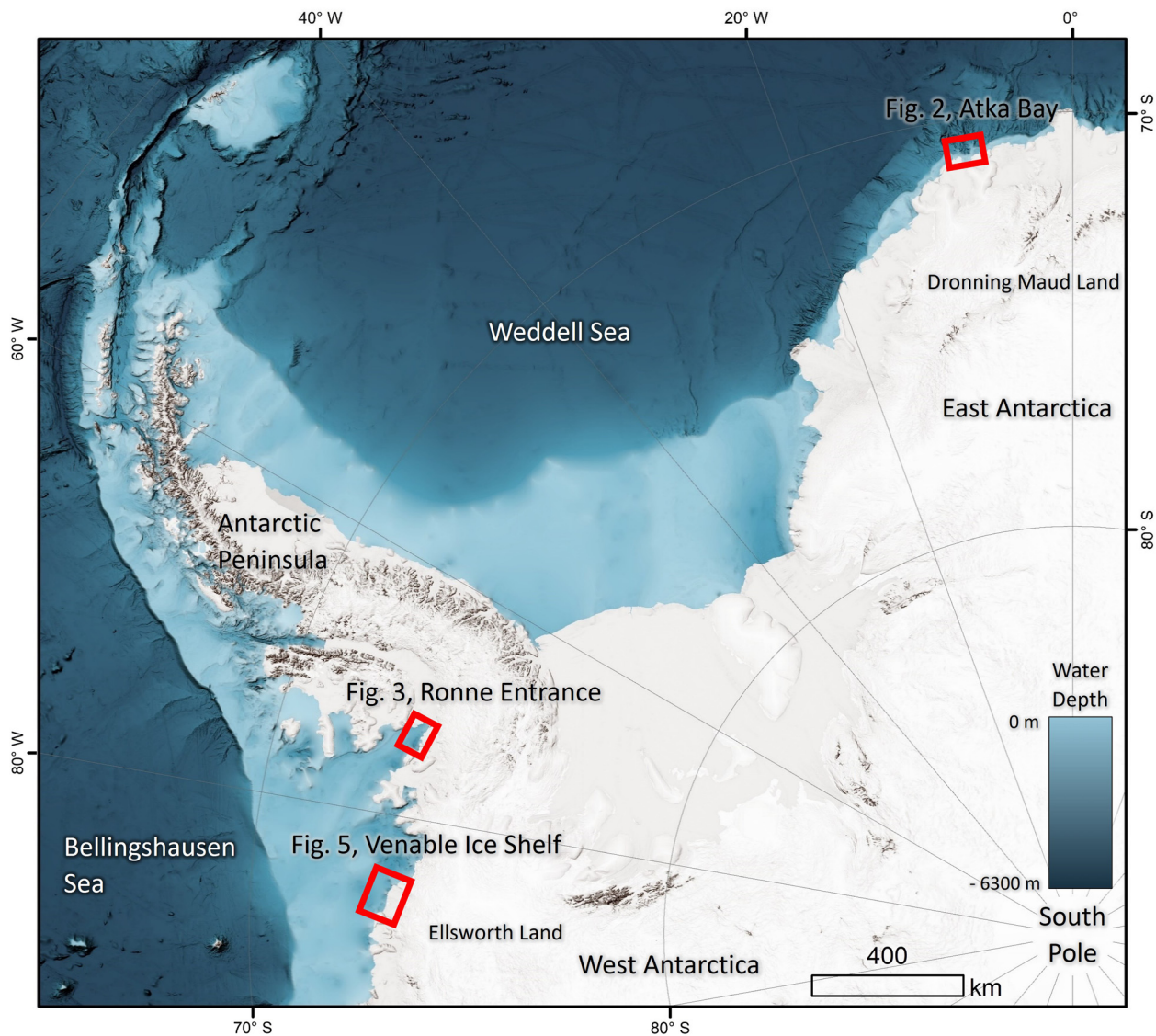


**Figure 1.** Overview map. Study areas are marked by red boxes. Background image is the International Bathymetric Chart of the Southern Ocean (IBCSO Version 2; Dorschel and others, 2022).

reductions in backscatter over larger regions (several kilometers), suggesting potential patterns that may be associated with meltwater presence rather than random variability. From this, a short-list of sites both traversed by the *RV Polarstern* and suspected of containing meltwater was established. Sigma nought-corrected radar backscatter values were averaged (mean) within 100 m along the shiptrack at positions where the ship crossed areas of low radar backscatter features emanating from ice shelves. To determine significant changes within the radar signal time series, changepoint detection was applied using the Pruned Exact Linear Time (PELT) algorithm (Killick and others, 2012; Killick and Eckley, 2014).

## 2.2 Measurement of water properties

Our shipboard data analysis focused on identifying anomalous cold and fresh water that could indicate the presence of meltwater (e.g. Jenkins, 1999; Pan and others, 2019). Water temperature and salinity were measured at a resolution of 1 s using two SBE21 thermo-salinographs and two auxiliary SBE38 temperature sensors, providing temperature measurements with an accuracy of  $\pm 0.001^\circ\text{C}$  and conductivity with an accuracy of  $\pm 0.001 \text{ S m}^{-1}$  (Sea-Bird Scientific, USA). The sensors are part

of an underway seawater flow-through system situated 11 m below the water surface on the ship's keel. The data were resampled by calculating the mean of 1 min intervals and any statistical outliers were removed. Sensor drift was also adjusted (Hoppmann and others, 2023a, 2023b). Salinity was calculated from the measured temperature, conductivity and pressure according to the PSS-78 Practical Salinity Scale (Hoppmann and others, 2023a, 2023b). Water temperature and salinity were then converted to conservative water temperature and absolute salinity in accordance with community standards using the Gibbs SeaWater oceanographic toolbox (McDougall and Barker, 2011). Positioning data were sourced from two Trimble SPS855 GPS receivers stationed on the ship's bridge, each paired with a Trimble Zephyr Model 2 Rugged Antenna (Trimble, USA) on the antenna deck above. The recorded data were then examined for the periods when the ship crossed the areas of suspected meltwater, as identified in the SAR imagery (Section 2.1). Additionally, wind speed and wind direction data were recorded via an Ultrasonic Anemometer Sonic 2D situated on the foremast at 39 m above sea level. Changes in these parameters can indicate if observations of surface water properties might be wind-influenced and otherwise falsely interpreted.



### 2.3 Helicopter survey of basal channel morphology and surface meltwater characteristics

To investigate and describe the morphology of the surface expression of basal channels and the characteristics of their expelled meltwater, a helicopter survey was conducted on 24 February 2023 along the face of Ferrigno and Fox ice streams and the Venable Ice Shelf in Ellsworth Land, West Antarctica (Fig. 1). Photographs taken in regular intervals with a Canon EOS 7D Mark II camera with a 50 mm  $f/1.4$  lens from the helicopter provided a unique opportunity for conducting detailed observations of the surface expression of basal channels, including their morphology, dimensions and their correlation with fractures on the ice shelf. GPS coordinates were recorded simultaneously to provide the location of each image. Additionally, anomalies in the surface water near the outflows of the basal channels – such as unusual coloration, turbidity or patterns of flow not typical of the surrounding water – were documented, aiming to link observations in SAR imagery with assumptions about meltwater properties and their radar backscatter characteristics.

## 3. Results

### 3.1 Site 1: Atka Bay off Ekström Ice Shelf

On 26 January 2022, expedition PS128 (Tiedemann and Müller, 2022) traversed Atka Bay, located to the north of the Ekström Ice Shelf in Dronning Maud Land, East Antarctica during a seismic survey. Sea ice and icebergs were almost completely absent from the bay during the survey (Fig. 2). The measuring period in Atka Bay lasted from 01.00 to 06.30 UTC, during which the ship maintained a consistent speed of 4.7 knots (over ground), covering a distance of  $\sim 45$  km.

Sentinel-1A SAR imagery captured on 25 January 2022 at 21.00 UTC reveals an area of distinctive low backscatter extending from the eastern side of the Ekström Ice Shelf, following a curved path northeastward for  $\sim 40$  km (Fig. 2a). The imagery was acquired in Extra Wide Swath (EW) beam mode 3 with horizontal–horizontal polarization and processed as a Ground Range Detected (GRDM) image. The incidence angle range was  $32.65$ – $39.66^\circ$  and the range and azimuth resolution are 20 and 40 m, respectively. During the survey, the low radar backscatter structure was crossed twice, at distances of  $\sim 15$  and  $\sim 29$  km along the shiptrack. Here, sigma nought-corrected radar backscatter values, quantifying the radar energy reflected back to the sensor, dropped significantly – as determined by the PELT algorithm (Supplementary Fig. 1) – from  $\sim -22$  to  $-35$  dB (Figs 2b, c).

Over the initial 15 km along the shiptrack (102 min), the water temperature and salinity remained stable, with means of  $-1.50^\circ\text{C}$  (std dev.,  $\sigma = 0.01^\circ\text{C}$ ) and  $33.85 \text{ g kg}^{-1}$  ( $\sigma = 0.007 \text{ g kg}^{-1}$ ), respectively. A non-parametric Mann–Whitney  $U$  test (Mann and Whitney, 1947; Wilcoxon, 1992) reveals that both parameters experienced statistically significant reductions ( $p < 0.001$ ) when entering the area of low radar backscatter extending from the Ekström Ice Shelf at  $\sim 15$ – $20.5$  km along the shiptrack (Figs 2 and 4). Here, water temperatures decreased to a mean of  $-1.56^\circ\text{C}$  ( $\sigma = 0.04^\circ\text{C}$ ), and salinity to a mean of  $33.79 \text{ g kg}^{-1}$  ( $\sigma = 0.02 \text{ g kg}^{-1}$ ). After the ship exited the area of low radar backscatter (Fig. 2b), water temperature and salinity returned to higher mean values of  $-1.47^\circ\text{C}$  ( $\sigma = 0.01^\circ\text{C}$ ) and  $33.82 \text{ g kg}^{-1}$  ( $\sigma = 0.007 \text{ g kg}^{-1}$ ), respectively. The ship entered the area of low radar backscatter for a second time between 29 and 33.5 km along shiptrack, and water temperature again decreased to a mean of  $-1.56^\circ\text{C}$  ( $\sigma = 0.08^\circ\text{C}$ ). During this interval, the mean salinity was  $33.83 \text{ g kg}^{-1}$  ( $\sigma = 0.02 \text{ g kg}^{-1}$ ), though a significant low of  $33.77 \text{ g kg}^{-1}$  was recorded (Fig. 2c). Both parameters then returned

to their prior stable values. Wind direction and speed remained consistent throughout the measurement period (Fig. 2d).

### 3.2 Site 2: Ronne Entrance off George VI Ice Shelf

During a bathymetric survey on 21 January 2023, expedition PS134 (Gohl, 2023) traversed the Ronne Entrance – the broad southwestern entrance of the George VI Sound in the south-eastern Bellingshausen Sea, West Antarctica (Fig. 1). The measuring period spanned from 02.48 to 07.54 UTC, during which the ship maintained a mean speed of 7.8 knots (over ground), traversing 74 km. From  $\sim 20$  to 74 km the ship's course followed the southern extension of the George VI Ice Shelf, keeping a mean distance of  $\sim 7$  km from the ice-shelf front (Fig. 3). Sea ice and icebergs were almost completely absent from the bay during the survey and hence did not influence the measurements of water properties.

Sentinel-1A SAR imagery captured on 22 January 2023 at 07.23 UTC displays an area of low radar backscatter near a grounded ice mass adjoining the George VI Ice Shelf, extending  $\sim 13$  km outward (Figs 3a, d). The imagery was acquired in EW4 and EW5 modes with horizontal–horizontal polarization and processed as a GRDM image. The incidence angle range was  $37.84$ – $46.97^\circ$  and the range and azimuth resolution are 20 and 40 m, respectively. During the survey, the structure of low radar backscatter was crossed from  $\sim 22$  to 32 km along the shiptrack. Along this segment of the shiptrack, radar backscatter values decreased significantly – as determined by the PELT algorithm (Supplementary Fig. 2) – by  $\sim 8$ – $10$  dB (Fig. 3b). Unfortunately, the temporally closest SAR image available depicts a swath of sea ice covering the area from  $\sim 34$  to 46 km along the shiptrack. This sea ice was not present during the observation period; however, due to the opportunistic nature of this study, there was no flexibility to navigate this area at a different time or under alternative conditions, necessitating the use of the closest available Sentinel-1A SAR imagery that corresponds with the time of the crossing.

Throughout the measurement period, water temperatures ranged from  $0.34$  to  $1.73^\circ\text{C}$  and salinity levels from  $32.13$  to  $33.03 \text{ g kg}^{-1}$ . These fluctuations were notably more pronounced than those recorded in Atka Bay. For the first 22 km along the shiptrack, the mean water temperatures were  $1.16^\circ\text{C}$  ( $\sigma = 0.33^\circ\text{C}$ ), while the mean salinity was measured at  $32.71 \text{ g kg}^{-1}$  ( $\sigma = 0.22 \text{ g kg}^{-1}$ ). Both parameters experienced statistically significant reductions ( $p < 0.001$ ) when entering the area of low radar backscatter extending from the George VI Ice Shelf at  $\sim 22$ – $32$  km along the shiptrack (Figs 3 and 4). Here, mean water temperatures dropped to  $0.65^\circ\text{C}$  ( $\sigma = 0.09^\circ\text{C}$ ) and mean salinity to  $32.38 \text{ g kg}^{-1}$  ( $\sigma = 0.04 \text{ g kg}^{-1}$ ). Beyond 32 km along the shiptrack, water temperature and salinity levels had mean values of  $1.12^\circ\text{C}$  ( $\sigma = 0.29^\circ\text{C}$ ) and  $32.75 \text{ g kg}^{-1}$  ( $\sigma = 0.17 \text{ g kg}^{-1}$ ), respectively (Fig. 3b).

### 3.3 Site 3: Venable Ice Shelf

Expedition PS134 (Gohl, 2023) traveled along the front of Venable Ice Shelf on 24–25 February 2023, tracing a route roughly parallel to the ice-shelf front at a distance of 2.6–20 km from the ice margin (Supplementary Fig. 3). Numerous icebergs were located all along the ice shelf, necessitating a survey track further away from the ice-shelf front. Although Sentinel-1A SAR imagery from 23 and 25 February 2023 showed no distinct low radar reflectivity areas (Supplementary Fig. 3), a helicopter survey provided insights into meltwater processes at the ice-shelf front, offering context for interpreting observations at other locations.

The helicopter reconnaissance flight surveyed 190 km along the face of Ferrigno and Fox ice streams and the Venable Ice

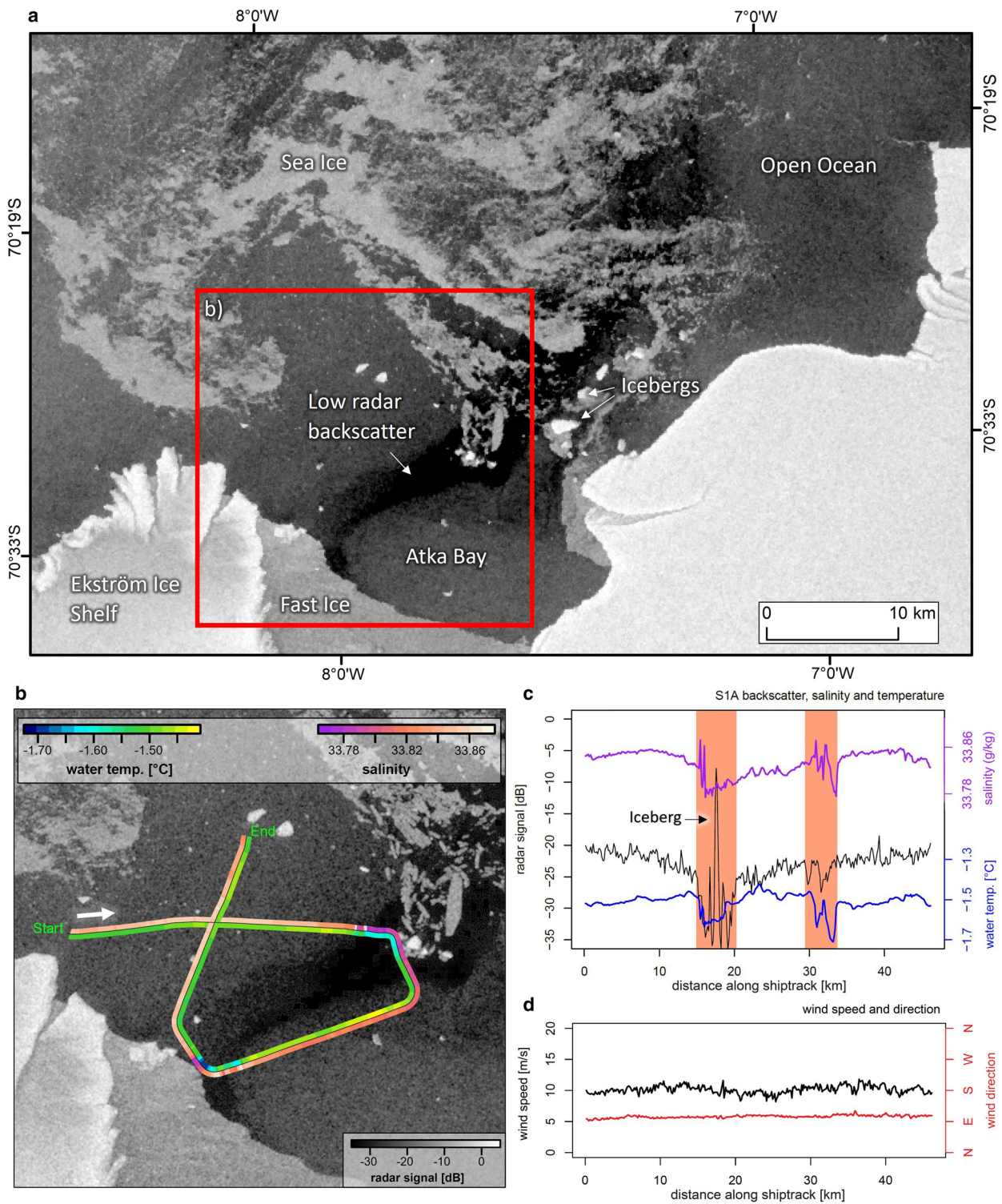


**Figure 2.** SAR and in situ data of Atka Bay. (a) Sentinel-1A SAR imagery of Atka Bay from 25 January 2022 at 21.00 UTC, showing a distinct feature of low radar backscatter extending ~40 km northeastward of the Ekström Ice Shelf. The study area is outlined in red. (b) The study area showing the ship's survey track (black line); water temperature data are represented to the right of the ship's track and salinity data to the left, relative to the ship's heading indicated by a white arrow. (c) Plots of radar backscatter signal, absolute salinity and conservative water temperature along the survey track. Segments coinciding with the low radar backscatter feature evident in (a) and (b) are highlighted. (d) Wind data plotted against the survey track.

Shelf (Fig. 5). Notable glaciological observations are plotted in Figure 5a. During a year of record low summer minimum sea-ice extent (Gilbert and Holmes, 2024), the calving front of the Venable Ice Shelf was one of the few places in the Bellingshausen Sea where remnants of sea ice remained, largely clustered in local embayments or within rifts between the ice-shelf front and recently calved icebergs. Other regions of the ice-shelf front also contained large arch-like geometries, presumably

arising from basal crevassing or wave erosion action that may have been enhanced by the absence of sea ice, which plays a dampening role in wave action on the face of ice shelves (Christie and others, 2022) (Fig. 5b).

Satellite images reveal that the Venable Ice Shelf contains at least seven surficial expressions of basal channels extending up to 38 km inland from the ice-shelf front (Fig. 5a). Four of these channels were confidently identifiable during the helicopter



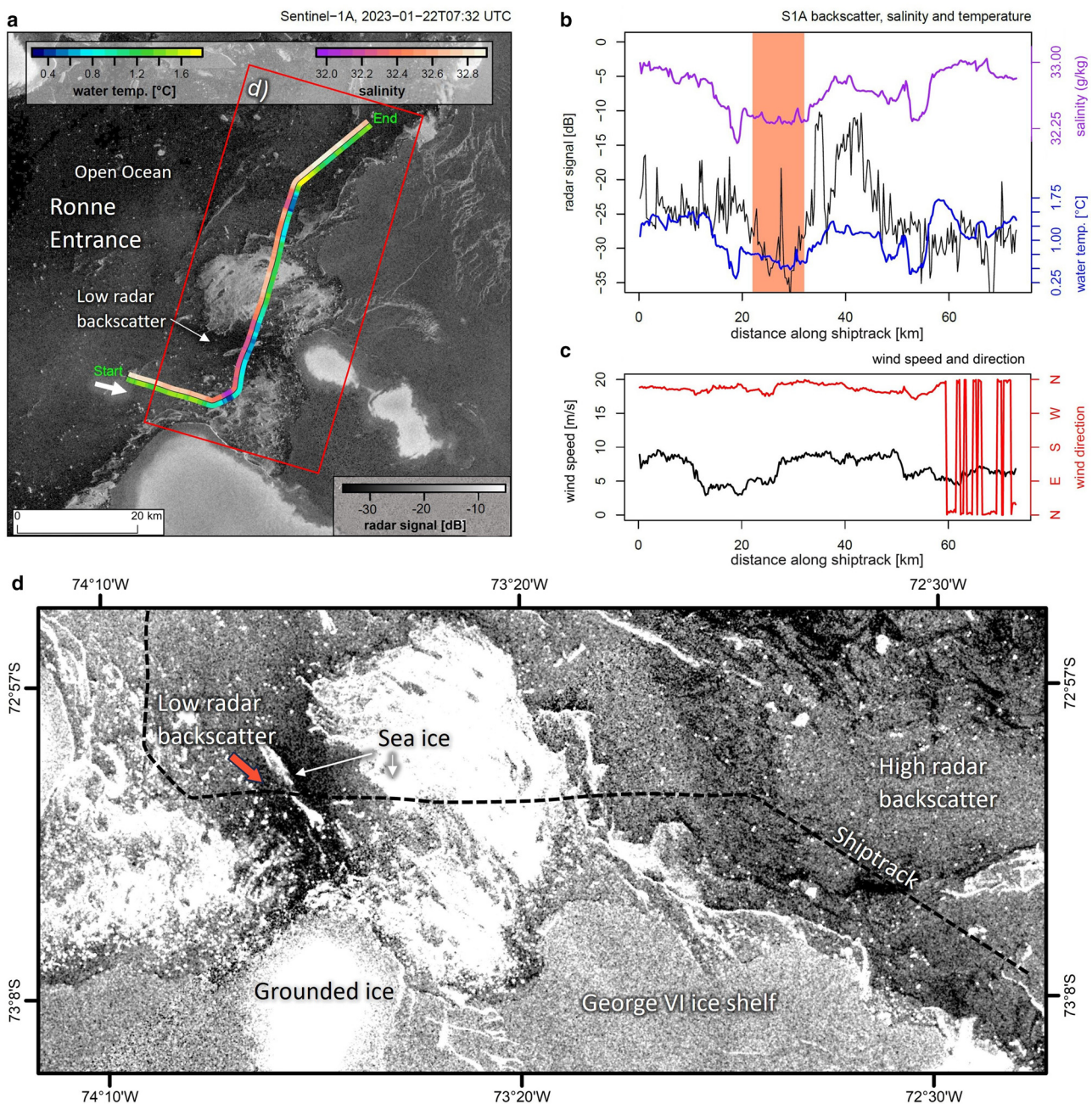


**Figure 3.** SAR and in situ data from Ronne Entrance. (a) Sentinel-1A SAR imagery of Ronne Entrance from 22 January 2023 at 07:32 UTC, showing the ship's survey track (black line); water temperature data are represented to the right of the ship's track and salinity data to the left, relative to the ship's heading indicated by a white arrow. (b) Plots of radar backscatter signal, absolute salinity and conservative water temperature along the survey track. The segment coinciding with a distinct low radar backscatter feature extending ~13 km outward from the George VI Ice Shelf is highlighted. (c) Wind data plotted against the survey track. (d) Zoomed-in section of the study area within the red square of (a), with enhanced contrast to better distinguish features. The dashed black line represents the ship's survey track. A red arrow identifies the area of low radar backscatter.

survey. Using the 8 m resolution Antarctic DEM (ESRI, 2020) to measure the width of the channels (with the channel edges defined as the point at which slope gradients exceed  $1^\circ$ ), we estimate that the channels were between 1032 and 1345 m wide at the ice-shelf front, with an average width of 1180 m. Viewed obliquely from the helicopter, it was apparent that the channels were characterized by a significant deviation in surface elevation compared to the remainder of the ice shelf (Figs 5c–e), with the ice-shelf surface reducing from ~50 m above the waterline to a minimum of ~12 m at the deepest point of the channel cross section. The channel cross sections were frequently asymmetric. In addition, several of the channels terminated in semicircular embayments set back by several hundred meters from the main ice-shelf

front (Figs 5c, e). Some channels were also associated with rifts opening perpendicular to the channel flanks (Fig. 5f).

The water properties in front of some of the channels also differed in character to the majority of the water in front of the remainder of the ice shelf. Most notably, at distances of ~30–40 m in front of the terminus of some of the largest basal channels some regions of the water surface were characterized by ribbons of a smooth, highly reflective water with a gloss-like texture (Figs 5f, g and Supplementary Fig. 4). These ribbon-like features spanned a width of ~10–50 m and differed in surficial appearance from both the turbulent and ruffled texture of areas of water disturbed by winds, and from calmer areas of water sheltered in the lee of katabatic winds directly adjacent to the ice shelf.

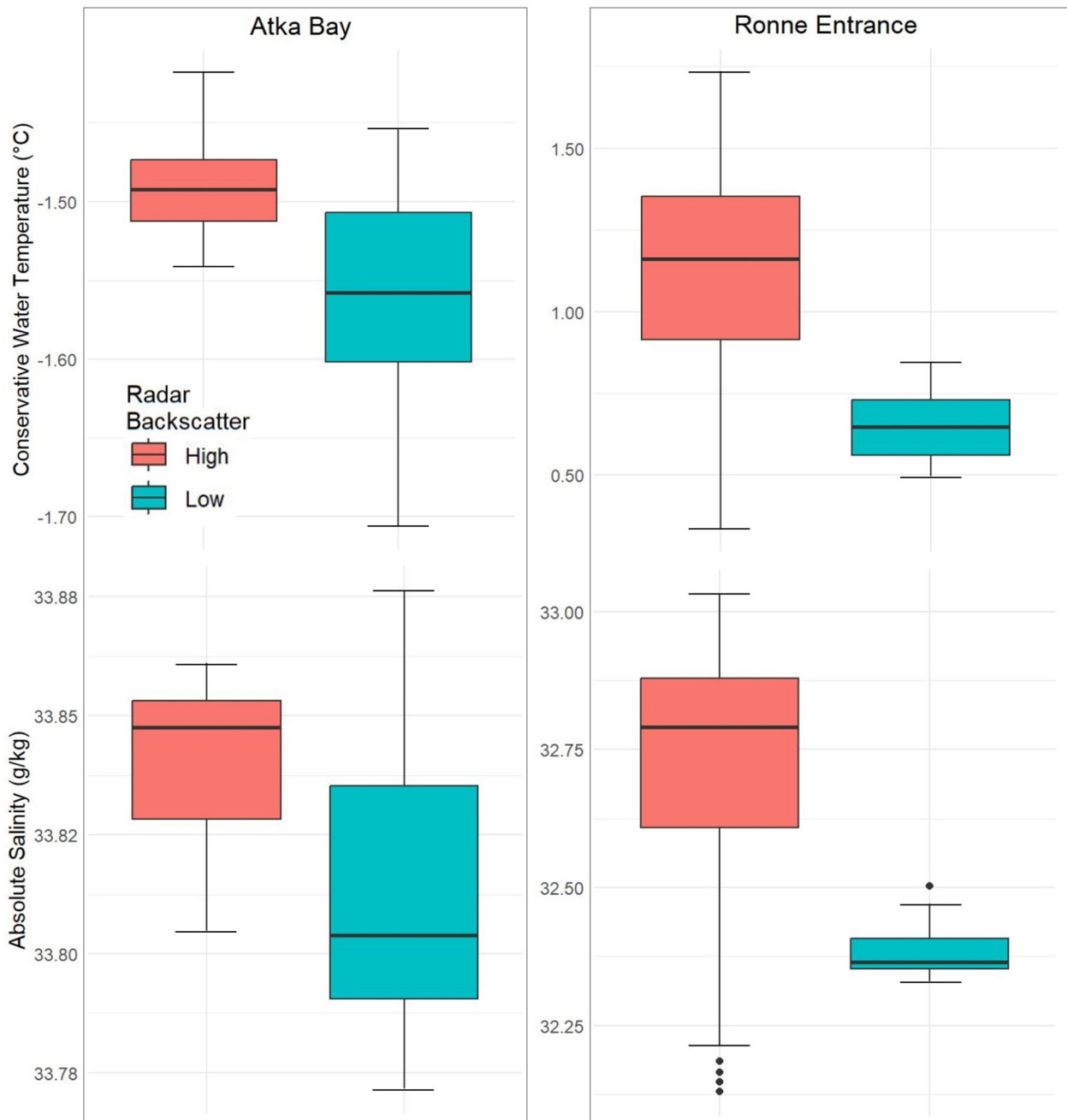


**Figure 4.** Comparative boxplot of water temperature (top) and salinity (bottom) measurements for Atka Bay (left) and Ronne Entrance (right). Red boxes represent measurements outside the low radar backscatter areas, as marked in Figures 2 and 3. Blue boxes represent measurements within these low backscatter areas. Each boxplot shows the median (central line), interquartile range (box) and whiskers extending to the smallest and largest values within 1.5 times the interquartile range from the quartiles. Outliers, if present, are displayed as diamonds outside the whiskers.

## 4. Discussion

### 4.1 Signatures of meltwater discharge in radar imagery

Using SAR-based observations and in situ measurements of water properties acquired immediately offshore of two Antarctic ice shelves, our findings suggest a correlation between areas of low radar backscatter in SAR imagery and the discharge of meltwater from beneath Antarctic ice shelves. The significant reductions in salinity and water temperature for the sites at Atka Bay and the Ronne Entrance align well with the presence of low radar backscatter areas observable in the closest available SAR imagery to our field observations.

Radar backscatter can be influenced by a multitude of factors including surface roughness, dielectric properties of the medium and the incidence angle of the radar signal. SAR imagery can

capture signatures of atmospheric and oceanic processes that affect the generation and modulation of short surface waves known as Bragg waves. This is because lower wind stress results in smoother surfaces and areas of relatively low radar backscatter as the radar's microwave pulse is reflected away from the sensor (e.g. Phillips, 1988; Kudryavtsev and others, 2005; Elyouncha and others, 2021).

Sea surface temperature boundaries have been observed to drive changes in the stability of the air–sea interface, which can also cause low radar backscatter in SAR imagery (Kozlov and others, 2012; Gurova and others, 2013). Cold upwelling water at the ocean surface often creates sea surface temperature boundaries and cools the overlying air, enhancing the stability of the marine atmospheric boundary layer by limiting vertical mixing through an increased atmospheric density contrast and more stable



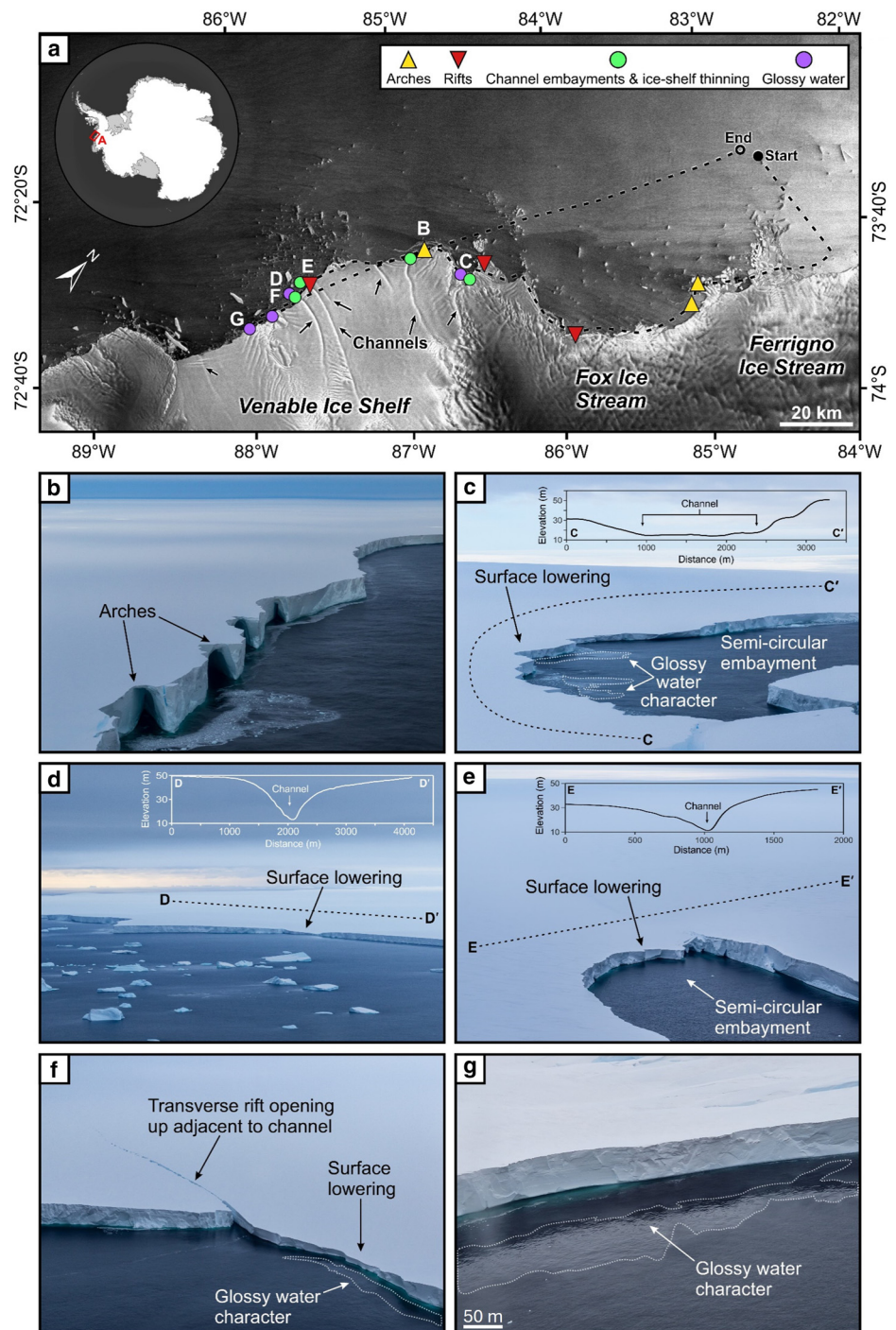


**Figure 5.** Observations made during the helicopter survey of Venable Ice Shelf. (a) Overview map displaying the GPS track of the helicopter survey along the face of the Venable Ice Shelf and the Fox and Ferrigno ice streams and associated glaciological observations. (b) Arches observed along the face of Venable Ice Shelf. (c–f) Photographs of the surface expression of basal channels present on the Venable Ice Shelf, exhibiting substantial surface lowering compared to the surrounding ice-shelf surface (d), semicircular embayments at the channel terminus (c, e) and transverse rifts opening adjacent to the channel (f). (g) Ribbons of glossy water.

temperature stratification (Friehe and others, 1991; Beal and others, 1997). Additionally, current shear in oceanic water, caused by differing flow velocities, can disrupt the energy transfer needed to maintain or generate larger waves, leading to low radar backscatter (Johannessen and others, 1996). The differences in water density and surface tension then create areas of the sea surface that are smoother than the surrounding water (e.g. Ermakov and others, 1992; Garabetian and others, 1993).

Similarly, the relatively cold, low-salinity upwelled water produced from the basal melting of ice shelves, being more buoyant than the surrounding sea water, can stabilize the temperature gradient within the marine atmospheric boundary layer at the air–sea interface, reducing vertical mixing. The lower salinity meltwater further enhances this stability by increasing the density contrast, lowering surface density and promoting vertical stability within

the upper water column. When this buoyant meltwater plume interacts with surface water of varying current speeds or directions, it can induce shear and modulate wave propagation (Fig. 6). The stratified and stabilized surface layer, along with the potential for increased nutrient loading from the meltwater (Arrigo and others, 2015), can furthermore stimulate phytoplankton growth and accumulation (Smith and Nelson, 1985; Ducklow and others, 2013), potentially creating a smooth biogenic surface film (e.g. Gade and others, 1998; Gade and others, 2013). These stabilizing effects reduce wind stress and decrease Bragg scattering waves, leading to lower radar backscatter (Fig. 6). When not influenced by strong winds and currents, these distinct water masses can be detected in SAR imagery (Figs 2 and 3).

For the visibility of these effects in SAR imagery, low and consistent wind speeds are generally required to clearly observe the



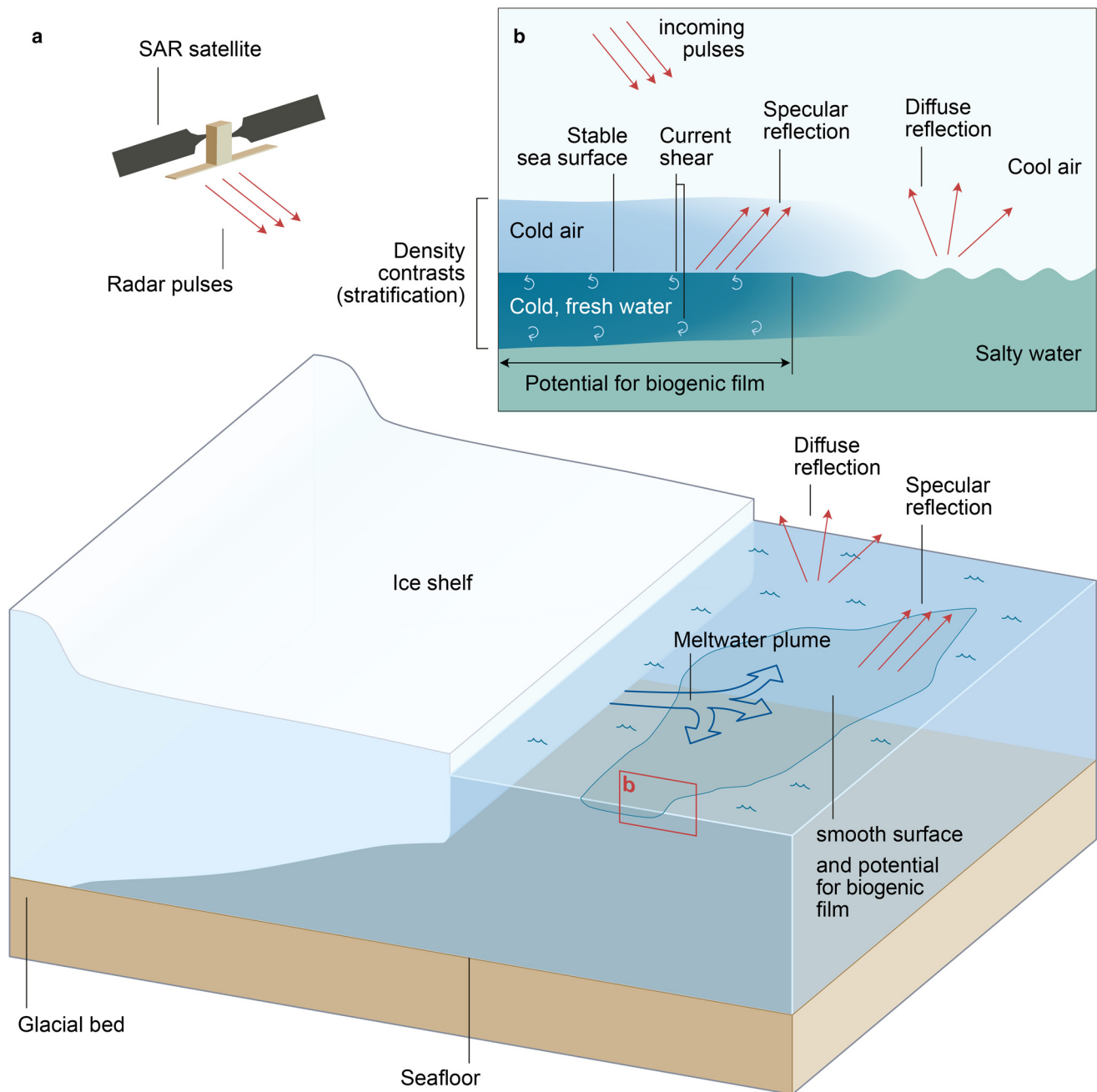


**Figure 6.** Proposed mechanism to account for the reduced radar backscatter signature of meltwater outflows. (a) 3-D representation of an ice shelf undergoing basal melting and the resultant differing radar reflection of meltwater and sea water. (b) 2-D cross section for the area within the red square in (a), showing the interface between cold, fresh meltwater and warmer, saltier sea water, along with the corresponding radar reflection.

wave-dampening effects without interference from stronger atmospheric disturbances (Handler and others, 2001; Kozlov and others, 2012). Fortunately, wind speed and direction data did not vary considerably for either Atka Bay or Ronne Entrance (Figs 2d and 3c). Both wind speed and direction did change along the Venable Ice Shelf transect however, which alongside the non-concurrent SAR image for the time of the transect and the complex cover of icebergs, may provide a possible explanation why no distinct low radar reflectivity areas were detected at this location (Supplementary Fig. 3).

In addition, as upwelling meltwater remains confined to the area adjacent to the ice margin, both temperature and salinity differences decrease with distance, leading to a reduction in current shear and stratification at the air–sea interface. Consequently, with increasing distance from the ice, it should become more

difficult to assess meltwater-induced low radar backscattering. Determining the spatial scales over which such signatures in SAR can occur solely from meltwater plumes is difficult. However, at the most convincing site at Atka Bay, the low radar backscatter structure extends distinctly for ~40 km. Hence, it can be assumed that such structures, similar to other upwelling-induced low radar backscatter, can extend for many tens of kilometers at least.

It is important to note that the appearance of specular radar reflection on water surfaces can be influenced by other factors that contribute to wave dampening, such as current shear in front of eddies (Johannessen and other, 1996; Karimova, 2012; Gade and others, 2013) as well as disturbances from wind and rain (Melsheimer and others, 1998). However, in the examples presented here, wind speed and direction remained constant,

and no rain or snowfall occurred. In the case of detecting specular radar reflection adjacent to ice shelves, katabatic winds can cause rough, wind-disturbed water surfaces away from the lee of the ice shelf. Therefore, it is important to consider local topography and the radar backscatter pattern when analyzing an ice-shelf proximal environment purely from a remote-sensing perspective. Moreover, the formation of a thin grease ice cover at the water surface can cause decreased radar backscatter compared to surrounding areas of open water due to its smooth surface and the dampening effect on waves caused by the physical barrier posed by the ice (e.g. Clemente-Colón and Yan, 2000; Kodaira and others, 2021). Such an effect would be more likely within polynyas and other areas of relatively calm water. No grease ice was observed during the observation periods at the three selected sites.

#### 4.2 Basal channel observations

The Venable Ice Shelf experienced the most pronounced thickness reduction of any ice shelf in Antarctica between 1994 and 2012 (Paolo and others, 2015). The surficial depressions visible on its surface reflect the hydrostatic relaxation of the overlying ice due to the formation of relatively large basal channels beneath the ice shelf (Le Brocq and others, 2013; Alley and others, 2022). Previous work has demonstrated that these basal channels occur where plumes of buoyant meltwater melt troughs into the ice-shelf base (e.g. Le Brocq and others, 2013; Drews, 2015; Alley and others, 2016; Alley and others, 2022; Alley and others, 2024). The largest channels are frequently associated with high basal melt rates – especially those directly influenced by modified Circumpolar Deep Water (e.g. Alley and others, 2016). This association has been strengthened in the case of the Venable Ice Shelf channels by Alley and others (2024), who report that several channels have become straighter over time, suggesting that they are likely moving toward a form of steady state driven by ocean warming. The development of basal channels can also concentrate the thinning and structural weakening of ice shelves, affecting their stability (Dow and others, 2018; Alley and others, 2019).

Our helicopter-based observations support many previous inferences made from satellite-based measurements such as substantial reductions in the ice-shelf surface height (typically from 50 to ~12 m above the waterline) (Figs 5c–e), and their association with enhanced transverse fracturing (Fig. 5f) (Dow and others, 2018; Alley and others, 2019). We speculate that the current semicircular embayment-like form of several of the channel outlets – set back by several hundred meters from the main ice-shelf front (Figs 5c, e) – reflects part of the lifecycle of this enhanced ice-shelf transverse fracturing, whereby greater ice-shelf thinning and melting lead to embayment formation, exposing the flanks of the embayment to greater mechanical weakening, enhanced fracturing and more frequent calving events (Alley and others, 2019). Additionally, cross sections of channels on the surface of the Venable Ice Shelf (Figs 5c–e) exhibit steeper slopes on the Coriolis-favored side, aligning with previous observations that Coriolis deflection leads to higher basal melt rates and asymmetric melt patterns of basal channels in Antarctic ice shelves (Sergienko, 2013; Alley and others, 2016, 2024).

The ribbons of smooth, highly reflective water observed close to the outlet of several, but not all, channels (Figs 5a, c, f, g and Supplementary Fig. 4) are too small to be adequately captured in Sentinel-1A SAR imagery. However, we speculate that these glossy water surfaces may represent smaller-scale examples of our proposed mechanism for the lower radar backscatter over relatively fresh water, indicating meltwater presence: a smooth water surface layer stabilized by temperature and salinity contrasts with the surrounding ocean water. The areas of glossy water were associated with some of the largest basal channels, where theory suggests

that higher melt rates are more likely (Alley and others, 2016); this hypothesis is supported by water temperature and salinity measurements made in a nearby transect by *RV Polarstern*, as these areas had the lowest water temperature and salinity readings during the transect (Supplementary Fig. 3). We also rule out wind stress as a possible causal factor as the ribbons were observed at a distance from the ice-shelf front, and the intervening water surface had a different texture. A high meltwater flux could produce such a thin melt-enriched surface layer, which induces current shear and exhibits different physical properties than the surrounding water. It follows that the glossy, smooth water surfaces likely represent areas where meltwater upwelling is strongest. Less vigorous upwelling in the surrounding areas and the presence of relatively fresh, meltwater-enriched water on larger scales may therefore be analogous to what we observe as the low radar backscatter signature. We note, however, that our hypothesis to explain the small ribbon-like water textures present in front of some channels requires further testing – likely involving direct water sampling of similar features – to accurately validate.

#### 4.3 Implications and future directions

Our findings indicate the potential of SAR data as an approach to identify meltwater discharges from beneath Antarctic ice shelves. SAR technology offers all-weather and day-and-night imaging capabilities, making it a potentially valuable tool for monitoring meltwater dynamics in Antarctica. However, because wind, precipitation, sea ice and current shear in front of eddies can also affect radar backscatter (Johannessen and others, 1996; Melsheimer and others, 1998), thorough contextual analysis and additional data are crucial when using SAR imagery to study meltwater dynamics in Antarctica. It is also crucial to consider that radar backscattering is influenced by the specific parameters of the radar image. Higher frequencies, like X- and C-bands, capture detailed textural features that can indicate meltwater presence but are more susceptible to atmospheric disturbances (e.g. Xie and others, 2019). Polarization also affects detection, with horizontal polarization providing stronger returns from smooth water surfaces, and vertical polarization better detecting rough surfaces and texture changes. Furthermore, the incidence angle impacts sensitivity to surface features; lower angles enhance detection with stronger backscatter, while higher angles result in weaker signals and greater sensitivity to geometric and dielectric properties (e.g. Topouzelis and others, 2016; Chen and others, 2022).

In addition to remote-sensing techniques, it is also important to undertake in situ target sampling – such as CTD measurements – of water properties from meltwater discharges in Antarctica. This will not only contribute to improving understanding of the processes captured in the geological record relating to meltwater expulsion (e.g. the sedimentary deposits of meltwater plumes; Lepp and others, 2022; Clark and others, 2024) but will also enable a better quantification and correlation of the detected radar signatures with meltwater properties. To advance our understanding further, future research should prioritize expanding the application of radar-based meltwater detection techniques to more ice shelves, ideally with temporally concurrent sampling of water mass properties. Once fully established, machine learning techniques could then utilize SAR data to provide unsupervised monitoring of the export of basal meltwater at an ice-sheet-wide scale. Long-term observations would help to establish comprehensive meltwater databases for Antarctic ice shelves, detect trends, understand interannual variability and assess the impact of climate change on meltwater dynamics. Such data will be important in refining models, validating other remote-sensing techniques, and providing a baseline for future comparative studies.



**Supplementary material.** The supplementary material for this article can be found at <https://doi.org/10.1017/jog.2024.71>.

**Data.** Continuous thermo-salinograph measurements from PS128 and PS134 are available online at <https://doi.org/10.1594/PANGAEA.952425> and <https://doi.org/10.1594/PANGAEA.964292>, respectively (Hoppmann and others, 2023a, 2023b).

**Acknowledgements.** We thank the master and crew of *RV Polarstern* for their support in conducting expeditions PS128 and PS134. Funding for the expeditions and this project was contributed by the AWI research program 'Changing Earth-Sustaining our Future' in Subtopics 2.1 'Warming Climates' and 2.3 'Sea Level Change'. Expedition grant Nos. were AWI\_PS128\_4 and AWI\_PS134\_1. James David Kirkham was supported by the Natural Environment Research Council – British Antarctic Survey Polar Science for Planet Earth program. We thank Robert Larter for his valuable insights and discussions on the topic of the manuscript, as well as Simon Dreutter and Sandra Tippenhauer for their assistance with data analyses. We also thank three anonymous reviewers for their constructive comments. This study contributes to the Scientific Research Program 'Instabilities and Thresholds in Antarctica' (INSTANT) of the Scientific Committee for Antarctic Research (SCAR).

## References

- Adusumilli S, Fricker HA, Medley B, Padman L and Siegfried MR (2020) Interannual variations in meltwater input to the Southern Ocean from Antarctic ice shelves. *Nature Geoscience* **13**(9), 616–620. doi: [10.1038/s41561-020-0616-z](https://doi.org/10.1038/s41561-020-0616-z)
- Alley KE, Scambos TA, Siegfried MR and Fricker HA (2016) Impacts of warm water on Antarctic ice shelf stability through basal channel formation. *Nature Geoscience* **9**(4), 290–293. doi: [10.1038/ngeo2675](https://doi.org/10.1038/ngeo2675)
- Alley KE, Scambos TA, Alley RB and Holschuh N (2019) Troughs developed in ice-stream shear margins precondition ice shelves for ocean-driven breakup. *Science Advances* **5**(10), eaax2215. doi: [10.1126/sciadv.aax2215](https://doi.org/10.1126/sciadv.aax2215)
- Alley KE, Scambos TA and Alley RB (2022) The role of channelized basal melt in ice-shelf stability: recent progress and future priorities. *Annals of Glaciology* **63**(87–89), 18–22. doi: [10.1017/aog.2023.5](https://doi.org/10.1017/aog.2023.5)
- Alley KE and 12 others (2024) Evolution of sub-ice-shelf channels reveals changes in ocean-driven melt in West Antarctica. *Journal of Glaciology*, 1–15. doi: [10.1017/jog.2024.20](https://doi.org/10.1017/jog.2024.20)
- Alpers W, Holt B and Zeng K (2017) Oil spill detection by imaging radars: challenges and pitfalls. *Remote Sensing of Environment* **201**, 133–147. doi: [10.1016/j.rse.2017.09.002](https://doi.org/10.1016/j.rse.2017.09.002)
- Arrigo KR, van Dijken GL and Strong AL (2015) Environmental controls of marine productivity hot spots around Antarctica. *Journal of Geophysical Research: Oceans* **120**(8), 5545–5565. doi: [10.1002/2015JC010888](https://doi.org/10.1002/2015JC010888)
- Beal RC and 6 others (1997) The influence of the marine atmospheric boundary layer on ERS 1 synthetic aperture radar imagery of the Gulf Stream. *Journal of Geophysical Research: Oceans* **102**(C3), 5799–5814. doi: [10.1029/96jc03109](https://doi.org/10.1029/96jc03109)
- Bronslaer B and 7 others (2018) Change in future climate due to Antarctic meltwater. *Nature* **564**(7734), 53–58. doi: [10.1038/s41586-018-0712-z](https://doi.org/10.1038/s41586-018-0712-z)
- Cazenave A and 89 others (2018) Global sea-level budget 1993–present. *Earth System Science Data* **10**(3), 1551–1590. doi: [10.5194/essd-10-1551-2018](https://doi.org/10.5194/essd-10-1551-2018)
- Chen X, Li G, Chen Z, Ju Q and Cheng X (2022) Incidence angle normalization of dual-polarized Sentinel-1 backscatter data on Greenland ice sheet. *Remote Sensing* **14**(21), 5534. doi: [10.3390/rs14215534](https://doi.org/10.3390/rs14215534)
- Christie FD and 5 others (2022) Antarctic ice-shelf advance driven by anomalous atmospheric and sea-ice circulation. *Nature Geoscience* **15**(5), 356–362. doi: [10.1038/s41561-022-00938-x](https://doi.org/10.1038/s41561-022-00938-x)
- Clark RW and 16 others (2024) Synchronous retreat of Thwaites and Pine Island glaciers in response to external forcings in the presatellite era. *Proceedings of the National Academy of Sciences of the United States of America* **121**(11), e2211711120. doi: [10.1073/pnas.2211711120](https://doi.org/10.1073/pnas.2211711120)
- Clemente-Colón P and Yan XH (2000) Low-backscatter ocean features in synthetic aperture radar imagery. *Johns Hopkins APL Technical Digest* **21**(1), 116–121.
- Cowton T, Nienow P, Bartholomew I, Sole A and Mair D (2012) Rapid erosion beneath the Greenland ice sheet. *Geology* **40**(4), 343–346. doi: [10.1130/G32687.1](https://doi.org/10.1130/G32687.1)
- Depoorter MA and 6 others (2013) Calving fluxes and basal melt rates of Antarctic ice shelves. *Nature* **502**(7469), 89–92. doi: [10.1038/nature12567](https://doi.org/10.1038/nature12567)
- Dirscherl M, Dietz AJ, Kneisel C and Kuenzer C (2021) A novel method for automated supraglacial lake mapping in Antarctica using Sentinel-1 SAR imagery and deep learning. *Remote Sensing* **13**(2), 197. doi: [10.3390/rs13020197](https://doi.org/10.3390/rs13020197)
- Dorschel B and 60 others (2022) The international bathymetric chart of the Southern Ocean version 2. *Scientific Data* **9**(1), 275. doi: [10.1038/s41597-022-01366-7](https://doi.org/10.1038/s41597-022-01366-7)
- Dow CF and 7 others (2018) Basal channels drive active surface hydrology and transverse ice shelf fracture. *Science Advances* **4**(6), ea07212. doi: [10.1126/sciadv.aao7212](https://doi.org/10.1126/sciadv.aao7212)
- Drews R (2015) Evolution of ice-shelf channels in Antarctic ice shelves. *The Cryosphere* **9**(3), 1169–1181. doi: [10.5194/tcd-9-1603-2015](https://doi.org/10.5194/tcd-9-1603-2015)
- Ducklow H and 11 others (2013) West Antarctic Peninsula: an ice-dependent coastal marine ecosystem in transition. *Oceanography* **26**(3), 190–203. doi: [10.5670/oceanog.2013.62](https://doi.org/10.5670/oceanog.2013.62)
- Dupont TK and Alley RB (2005) Assessment of the importance of ice-shelf buttressing to ice-sheet flow. *Geophysical Research Letters* **32**(4), L04503. doi: [10.1029/2004gl022024](https://doi.org/10.1029/2004gl022024)
- Elyouncha A, Eriksson LE, Broström G, Axell L and Ulander LH (2021) Joint retrieval of ocean surface wind and current vectors from satellite SAR data using a Bayesian inversion method. *Remote Sensing of Environment* **260**, 112455. doi: [10.1016/j.rse.2021.112455](https://doi.org/10.1016/j.rse.2021.112455)
- Ermakov SA, Salashin SG and Panchenko AR (1992) Film slicks on the sea surface and some mechanisms of their formation. *Dynamics of Atmospheres and Oceans* **16**(3–4), 279–304. doi: [10.1016/0377-0265\(92\)90010-Q](https://doi.org/10.1016/0377-0265(92)90010-Q)
- ESRI (2020) Antarctic digital elevation model (DEM). Available at <https://www.arcgis.com/home/item.html?id=af22b667859b411993ac6094c1022ebc>
- Fricker HA and 12 others (2021) ICESat-2 meltwater depth estimates: application to surface melt on Amery Ice Shelf, East Antarctica. *Geophysical Research Letters* **48**(8), e2020GL090550. doi: [10.1029/2020GL090550](https://doi.org/10.1029/2020GL090550)
- Friehe CA and 9 others (1991) Air–sea fluxes and surface layer turbulence around a sea surface temperature front. *Journal of Geophysical Research: Oceans* **96**(C5), 8593–8609. doi: [10.1029/90JC02062](https://doi.org/10.1029/90JC02062)
- Fürst JJ and 6 others (2016) The safety band of Antarctic ice shelves. *Nature Climate Change* **6**(5), 479–482. doi: [10.1038/nclimate2912](https://doi.org/10.1038/nclimate2912)
- Gade M, Alpers W, Hühnerfuss H, Masuko H and Kobayashi T (1998) Imaging of biogenic and anthropogenic ocean surface films by the multifrequency/multipolarization SIR-C/X-SAR. *Journal of Geophysical Research: Oceans* **103**(C9), 18851–18866. doi: [10.1029/97jc01915](https://doi.org/10.1029/97jc01915)
- Gade M, Byfield V, Ermakov S, Lavrova O and Mitnik I (2013) Slicks as indicators for marine processes. *Oceanography* **26**(2), 138–149. doi: [10.5670/oceanog.2013.39](https://doi.org/10.5670/oceanog.2013.39)
- Garabetian F, Romano JC, Paul R and Sigoillot JC (1993) Organic matter composition and pollutant enrichment of sea surface microlayer inside and outside slicks. *Marine Environmental Research* **35**(4), 323–339. doi: [10.1016/0141-1136\(93\)90100-E](https://doi.org/10.1016/0141-1136(93)90100-E)
- Gilbert E and Holmes C (2024) 2023's Antarctic sea ice extent is the lowest on record. *Weather* **79**(2), 46–51. doi: [10.1002/wea.4518](https://doi.org/10.1002/wea.4518)
- Gladish CV, Holland DM, Holland PR and Price SF (2012) Ice-shelf basal channels in a coupled ice/ocean model. *Journal of Glaciology* **58**(212), 1227–1244. doi: [10.3189/2012jogG11J018](https://doi.org/10.3189/2012jogG11J018)
- Gohl K (ed.) (2023) The expedition PS134 of the research vessel POLARSTERN to the Bellinghousen Sea in 2022/2023. *Berichte zur Polar- und Meeresforschung/Reports on Polar and Marine Research* **777**, 181.
- Greene CA, Gardner AS, Schlegel NJ and Fraser AD (2022) Antarctic calving loss rivals ice-shelf thinning. *Nature* **609**(7929), 948–953. doi: [10.1038/s41586-022-05037-w](https://doi.org/10.1038/s41586-022-05037-w)
- Gudmundsson GH (2013) Ice-shelf buttressing and the stability of marine ice sheets. *The Cryosphere* **7**(2), 647–655. doi: [10.5194/tc-7-647-2013](https://doi.org/10.5194/tc-7-647-2013)
- Gunn KL, Rintoul SR, England MH and Bowen MM (2023) Recent reduced abyssal overturning and ventilation in the Australian Antarctic Basin. *Nature Climate Change* **13**(6), 537–544. doi: [10.1038/s41558-023-01667-8](https://doi.org/10.1038/s41558-023-01667-8)
- Gurova ES and Ivanov AY (2011) Appearance of sea surface signatures and current features in the South-East Baltic Sea on the MODIS and SAR images. *Issledovanie Zemli iz Kosmosa* **4**, 41–54 (in Russian).
- Gurova E, Lehmann A and Ivanov A (2013) Upwelling dynamics in the Baltic Sea studied by a combined SAR/infrared satellite data and circulation model analysis. *Oceanologia* **55**(3), 687–707. doi: [10.5697/oc.55-3.687](https://doi.org/10.5697/oc.55-3.687)
- Handler RA, Smith GB and Leighton RI (2001) The thermal structure of an air–water interface at low wind speeds. *Tellus A* **53**(2), 233–244. doi: [10.3402/tellusa.v53i2.12187](https://doi.org/10.3402/tellusa.v53i2.12187)

- Hoppmann M, Tippenhauer S and Tiedemann R** (2023a) Continuous thermosalinograph oceanography along RV *Polarstern* cruise track PS128. Alfred Wegener Institute, Helmholtz Centre for Polar and Marine Research, Bremerhaven, PANGAEA. doi: [10.1594/PANGAEA.952425](https://doi.org/10.1594/PANGAEA.952425)
- Hoppmann M, Tippenhauer S and Gohl K** (2023b) Continuous thermosalinograph oceanography along RV *Polarstern* cruise track PS134. Alfred Wegener Institute, Helmholtz Centre for Polar and Marine Research, Bremerhaven, PANGAEA. doi: [10.1594/PANGAEA.964292](https://doi.org/10.1594/PANGAEA.964292)
- Hudson B and 5 others** (2014) MODIS observed increase in duration and spatial extent of sediment plumes in Greenland fjords. *The Cryosphere* **8**(4), 1161–1176. doi: [10.5194/tc-8-1161-2014](https://doi.org/10.5194/tc-8-1161-2014)
- Jenkins A** (1999) The impact of melting ice on ocean waters. *Journal of Physical Oceanography* **29**(9), 2370–2381. doi: [10.1175/1520-0485\(1999\)029<2370>2.0.CO;2](https://doi.org/10.1175/1520-0485(1999)029<2370>2.0.CO;2)
- Jenkins A and 7 others** (2018) West Antarctic ice sheet retreat in the Amundsen Sea driven by decadal oceanic variability. *Nature Geoscience* **11**(10), 733–738. doi: [10.1038/s41561-018-0207-4](https://doi.org/10.1038/s41561-018-0207-4)
- Johannessen JA and 6 others** (1996) Coastal ocean fronts and eddies imaged with ERS 1 synthetic aperture radar. *Journal of Geophysical Research: Oceans* **101**(C3), 6651–6667. doi: [10.1029/95JC02962](https://doi.org/10.1029/95JC02962)
- Joughin I, Smith BE, Howat IM, Scambos T and Moon T** (2010) Greenland flow variability from ice-sheet-wide velocity mapping. *Journal of Glaciology* **56**(197), 415–430. doi: [10.3189/002214310792447734](https://doi.org/10.3189/002214310792447734)
- Karimova S** (2012) Spiral eddies in the Baltic, Black and Caspian seas as seen by satellite radar data. *Advances in Space Research* **50**(8), 1107–1124. doi: [10.1016/j.asr.2011.10.027](https://doi.org/10.1016/j.asr.2011.10.027)
- Kaufman YJ** (1984) Atmospheric effects on remote sensing of surface reflectance. *Remote Sensing: Critical Review of Technology* **475**, 20–33.
- Killick R and Eckley IA** (2014) ChangePoint: an R package for change-point analysis. *Journal of Statistical Software* **58**, 1–19. doi: [10.18637/jss.v058.i03](https://doi.org/10.18637/jss.v058.i03)
- Killick R, Fearnhead P and Eckley IA** (2012) Optimal detection of change-points with a linear computational cost. *Journal of the American Statistical Association* **107**(500), 1590–1598. doi: [10.1080/01621459.2012.737745](https://doi.org/10.1080/01621459.2012.737745)
- Kodaira T and 6 others** (2021) Observation of on-ice wind waves under grease ice in the western Arctic Ocean. *Polar Science* **27**, 100567. doi: [10.1016/j.polar.2020.100567](https://doi.org/10.1016/j.polar.2020.100567)
- Kozlov IE and 5 others** (2012) ASAR imaging for coastal upwelling in the Baltic Sea. *Advances in Space Research* **50**(8), 1125–1137. doi: [10.1016/j.asr.2011.08.017](https://doi.org/10.1016/j.asr.2011.08.017)
- Kudryavtsev V, Akimov D, Johannessen J and Chapron B** (2005) On radar imaging of current features: 1. Model and comparison with observations. *Journal of Geophysical Research: Oceans* **110**(C7), C07016. doi: [10.1029/2004jc002505](https://doi.org/10.1029/2004jc002505)
- Le Brocq AM and 10 others** (2013) Evidence from ice shelves for channelized meltwater flow beneath the Antarctic ice sheet. *Nature Geoscience* **6**(11), 945–948. doi: [10.1038/ngeo1977](https://doi.org/10.1038/ngeo1977)
- Lepp AP and 13 others** (2022) Sedimentary signatures of persistent subglacial meltwater drainage from Thwaites Glacier, Antarctica. *Frontiers in Earth Science* **10**, 863200. doi: [10.3389/feart.2022.863200](https://doi.org/10.3389/feart.2022.863200)
- Lewis SM and Smith LC** (2009) Hydrologic drainage of the Greenland ice sheet. *Hydrological Processes* **23**(14), 2004–2011. doi: [10.1002/hyp.7343](https://doi.org/10.1002/hyp.7343)
- Li W, Lhermitte S and López-Dekker P** (2021) The potential of synthetic aperture radar interferometry for assessing meltwater lake dynamics on Antarctic ice shelves. *The Cryosphere* **15**(12), 5309–5322. doi: [10.5194/tc-15-5309-2021](https://doi.org/10.5194/tc-15-5309-2021)
- Li Q, England MH, Hogg AM, Rintoul SR and Morrison AK** (2023) Abyssal ocean overturning slowdown and warming driven by Antarctic meltwater. *Nature* **615**(7954), 841–847. doi: [10.1038/s41586-023-05762-w](https://doi.org/10.1038/s41586-023-05762-w)
- Malek S, Melgani F, Bazi Y and Alajlan N** (2017) Reconstructing cloud-contaminated multispectral images with contextualized autoencoder neural networks. *IEEE Transactions on Geoscience and Remote Sensing* **56**(4), 2270–2282. doi: [10.1109/TGRS.2017.2777886](https://doi.org/10.1109/TGRS.2017.2777886)
- Mankoff KD, Jacobs SS, Tulaczyk SM and Stammerjohn SE** (2012) The role of Pine Island Glacier ice shelf basal channels in deep-water upwelling, polynyas and ocean circulation in Pine Island Bay, Antarctica. *Annals of Glaciology* **53**(60), 123–128. doi: [10.3189/2012AoG60A062](https://doi.org/10.3189/2012AoG60A062)
- Mann HB and Whitney DR** (1947) On a test of whether one of two random variables is stochastically larger than the other. *The Annals of Mathematical Statistics* **18**(1), 50–60.
- Markus T and Burns BA** (1993) Detection of coastal polynyas with passive microwave data. *Annals of Glaciology* **17**, 351–355. doi: [10.3189/S0260305500013094](https://doi.org/10.3189/S0260305500013094)
- McDougall TJ and Barker PM** (2011) Getting started with TEOS-10 and the Gibbs SeaWater (GSW) oceanographic toolbox. *SCOR/IAPSO WG 127*(532), 1–28.
- Melzheimer C, Alpers W and Gade M** (1998) Investigation of multifrequency/multipolarization radar signatures of rain cells over the ocean using SIR-C/X-SAR data. *Journal of Geophysical Research: Oceans* **103**(C9), 18867–18884. doi: [10.1029/98jc00779](https://doi.org/10.1029/98jc00779)
- Millgate T, Holland PR, Jenkins A and Johnson HL** (2013) The effect of basal channels on oceanic ice-shelf melting. *Journal of Geophysical Research: Oceans* **118**(12), 6951–6964. doi: [10.1002/2013jc009402](https://doi.org/10.1002/2013jc009402)
- Otosaka IN and 67 others** (2023) Mass balance of the Greenland and Antarctic ice sheets from 1992 to 2020. *Earth System Science Data* **15**(4), 1597–1616. doi: [10.5194/essd-15-1597-2023](https://doi.org/10.5194/essd-15-1597-2023)
- Pan BJ, Vernet M, Reynolds RA and Mitchell BG** (2019) The optical and biological properties of glacial meltwater in an Antarctic fjord. *PLoS ONE* **14**(2), e0211107. doi: [10.1371/journal.pone.0211107](https://doi.org/10.1371/journal.pone.0211107)
- Paolo FS, Fricker HA and Padman L** (2015) Volume loss from Antarctic ice shelves is accelerating. *Science* **348**(6232), 327–331. doi: [10.1126/science.aaa0940](https://doi.org/10.1126/science.aaa0940)
- Paolo FS and 6 others** (2023) Widespread slowdown in thinning rates of West Antarctic ice shelves. *The Cryosphere* **17**(8), 3409–3433. doi: [10.5194/tc-17-3409-2023](https://doi.org/10.5194/tc-17-3409-2023)
- Phillips OM** (1988) Radar returns from the sea surface – Bragg scattering and breaking waves. *Journal of Physical Oceanography* **18**(8), 1065–1074. doi: [10.1175/1520-0485\(1988\)018<1065:rrftss>2.0.co;2](https://doi.org/10.1175/1520-0485(1988)018<1065:rrftss>2.0.co;2)
- Pritchard H and 5 others** (2012) Antarctic ice-sheet loss driven by basal melting of ice shelves. *Nature* **484**(7395), 502–505. doi: [10.1038/nature10968](https://doi.org/10.1038/nature10968)
- Rignot E and Steffen K** (2008) Channelized bottom melting and stability of floating ice shelves. *Geophysical Research Letters* **35**(2), L02503. doi: [10.1029/2007GL031765](https://doi.org/10.1029/2007GL031765)
- Rignot E, Velicogna I, van den Broeke MR, Monaghan A and Lenaerts JT** (2011) Acceleration of the contribution of the Greenland and Antarctic ice sheets to sea level rise. *Geophysical Research Letters* **38**(5), L05503. doi: [10.1029/2011GL046583](https://doi.org/10.1029/2011GL046583)
- Rignot E, Jacobs S, Mouginot J and Scheuchl B** (2013) Ice-shelf melting around Antarctica. *Science* **341**(6143), 266–270. doi: [10.1126/science.1235798](https://doi.org/10.1126/science.1235798)
- Rignot E, Mouginot J, Morlighem M, Seroussi H and Scheuchl B** (2014) Widespread, rapid grounding line retreat of Pine Island, Thwaites, Smith, and Kohler glaciers, West Antarctica, from 1992 to 2011. *Geophysical Research Letters* **41**(10), 3502–3509. doi: [10.1002/2014GL060140](https://doi.org/10.1002/2014GL060140)
- Rignot E and 5 others** (2019) Four decades of Antarctic ice sheet mass balance from 1979–2017. *Proceedings of the National Academy of Sciences of the United States of America* **116**(4), 1095–1103. doi: [10.1073/pnas.1812883116](https://doi.org/10.1073/pnas.1812883116)
- Rignot E, Mouginot J, Scheuchl B and Jeong S** (2022) Changes in Antarctic ice sheet motion derived from satellite radar interferometry between 1995 and 2022. *Geophysical Research Letters* **49**(23), e2022GL100141. doi: [10.1029/2022gl100141](https://doi.org/10.1029/2022gl100141)
- Savidge E, Snow T and Siegfried MR** (2023) Multi-decadal record of sensible-heat polynya variability from satellite optical and thermal imagery at Pine Island Glacier, West Antarctica. *Geophysical Research Letters* **50**(22), e2023GL106178. doi: [10.1029/2023GL106178](https://doi.org/10.1029/2023GL106178)
- Scambos TA, Bohlander JA, Shuman CA and Skvarca P** (2004) Glacier acceleration and thinning after ice shelf collapse in the Larsen B embayment, Antarctica. *Geophysical Research Letters* **31**(18), L18402. doi: [10.1029/2004gl020670](https://doi.org/10.1029/2004gl020670)
- Schmidt BE and 28 others** (2023) Heterogeneous melting near the Thwaites Glacier grounding line. *Nature* **614**(7948), 471–478. doi: [10.1038/s41586-022-05691-0](https://doi.org/10.1038/s41586-022-05691-0)
- Schmidtko S, Heywood KJ, Thompson AF and Aoki S** (2014) Multidecadal warming of Antarctic waters. *Science* **346**(6214), 1227–1231. doi: [10.1126/science.1256117](https://doi.org/10.1126/science.1256117)
- Sergienko OV** (2013) Basal channels on ice shelves. *Journal of Geophysical Research: Earth Surface* **118**, 1342–1355. doi: [10.1002/jgrf.20105](https://doi.org/10.1002/jgrf.20105)
- Shepherd A and 79 others** (2018) Mass balance of the Antarctic ice sheet from 1992 to 2017. *Nature* **558**(7709), 219–222. doi: [10.1038/s41586-018-0179-y](https://doi.org/10.1038/s41586-018-0179-y)
- Smith WO and Nelson DM** (1985) Phytoplankton bloom produced by a receding ice edge in the Ross Sea: spatial coherence with the density field. *Science* **227**(4683), 163–166. doi: [10.1126/science.227.4683.163](https://doi.org/10.1126/science.227.4683.163)



- Stokes CR and 16 others** (2022) Response of the East Antarctic ice sheet to past and future climate change. *Nature* **608**(7922), 275–286. doi: [10.1038/s41586-022-04946-0](https://doi.org/10.1038/s41586-022-04946-0)
- Sundal AV and 5 others** (2011) Melt-induced speed-up of Greenland ice sheet offset by efficient subglacial drainage. *Nature* **469**(7331), 521–524. doi: [10.1038/nature09740](https://doi.org/10.1038/nature09740)
- Tedstone AJ and Arnold NS** (2012) Automated remote sensing of sediment plumes for identification of runoff from the Greenland ice sheet. *Journal of Glaciology* **58**(210), 699–712. doi: [10.3189/2012jog11j204](https://doi.org/10.3189/2012jog11j204)
- Tiedemann R and Müller J** (eds.) (2022) The Expedition PS128 of the Research Vessel *Polarstern* to the Weddell Sea, Lazarew Sea, Riiser-Larsen Sea, Cosmonaut Sea and Cooperation Sea in 2022. *Berichte zur Polar- und Meeresforschung/Reports on Polar and Marine Research*, 764, 235 p.
- Topouzelis K, Singha S and Kitsiou D** (2016) Incidence angle normalization of Wide Swath SAR data for oceanographic applications. *Open Geosciences* **8**(1), 450–464. doi: [10.1515/geo-2016-0029](https://doi.org/10.1515/geo-2016-0029)
- Ulaby FT, Moore RK and Fung AK** (1981) Microwave remote sensing: Active and passive. Volume 1 – Microwave remote sensing fundamentals and radiometry.
- Vaughan DG and 9 others** (2012) Subglacial melt channels and fracture in the floating part of Pine Island Glacier, Antarctica. *Journal of Geophysical Research: Earth Surface* **117**(F3), F03012. doi: [10.1029/2012jf002360](https://doi.org/10.1029/2012jf002360)
- Wilcoxon F** (1992) Individual comparisons by ranking methods. In *Breakthroughs in Statistics: Methodology and Distribution*. New York, NY: Springer, pp. 196–202. doi: [10.1007/978-1-4612-4380-9\\_16](https://doi.org/10.1007/978-1-4612-4380-9_16)
- Xie D, Chen KS and Zeng J** (2019) The frequency selective effect of radar backscattering from multiscale sea surface. *Remote Sensing* **11**(2), 160. doi: [10.3390/rs11020160](https://doi.org/10.3390/rs11020160)
- Zhu Z and Woodcock CE** (2014) Automated cloud, cloud shadow, and snow detection in multitemporal Landsat data: an algorithm designed specifically for monitoring land cover change. *Remote Sensing of Environment* **152**, 217–234. doi: [10.1016/j.rse.2014.06.012](https://doi.org/10.1016/j.rse.2014.06.012)